RSC Advances

ROYAL SOCIETY OF CHEMISTRY

www.rsc.org/advances

Journal Name

ARTICLE

Hydrothermal Synthesis and Enhanced Xylene-sensing Properties of Pompon-like Cr-doped Co_3O_4 Hierarchical Nanostructures

Received 00th January 20xx,
Accepted 00th January 20xx

DOI: 10.1039/x0xx00000x

www.rsc.org/

Yujia Li,[a] Xiaohui Ma,[a] Sijia Guo,[b] Bin Wang,[a] Dongming Sun,[c] Xindong Zhang[b,*] and Shengping Ruan[a,*]

Pompon-like Co_3O_4 and Cr-doped Co_3O_4 hierarchical nanostructures were synthesized via hydrothermal reaction, and a series of different proportions of Cr were doped to investigate the effect of Cr-doping on the gas sensing performance. All the prepared materials were used to fabricate gas sensors, and the result of their gas sensing properties measurement indicated that the optimum proportion of Cr/Co was 5 at%, whose response (6.38) to xylene (5 ppm) was higher than the other's. And with the increasing of Cr ratio, the response to xylene (5 ppm) tended to decline after ascending, taking 5 at% (Cr/Co) as the cut-off point, but all the sensors made by Cr-doped Co_3O_4 hierarchical nanostructures showed higher response to xylene than pure Co_3O_4 hierarchical nanostructures, which improved the selectivity of sensors. Besides, it was worth mentioning that all the sensors' optimum working temperatures were low, which required smaller heating current and low power consumption.

1. Introduction

The air is the most important element for people's life, but now the quality of air is increasingly deteriorating. Besides many factory chimneys and cars exhaust cylinders on the street, new furniture and paint also send out some harmful substances. As a representative of common indoor pollutant, excessive xylene can cause huge damage to human being and induce horrible diseases such as colon cancer, rectal cancer and lung cancer.[1] So air quality monitoring appears to be necessary for environmental sustainability and human people's health, and it is of great meaning to develop a reliable and effective gas sensor. There are a lot of detecting systems or methods to be applied in daily life and production, such as optical waveguide technique,[2] optical planar Bragg grating sensors,[3] biosensors,[4] chemical sensors,[5] and magnetoelastic sensors,[6] etc. Compared with them, gas sensors attract great attention due to their low cost, portability, convenient fabrication, and detectable possibility of large number of gases.[7]

As a typical metal oxide semiconductor (MOS), Co_3O_4 is used to apply in many fields for its extreme properties, including supercapacitor,[8] lithium-ion battery,[9, 10] energy storage,[11] electrochromic devices,[12] water oxidation,[13] catalysts,[14, 15] magnetic materials,[16] and gas sensor.[17, 18] As for gas-sensing application, Co_3O_4 nanostructures with different morphologies are prepared through various methods, such as nanocube prepared by microwave-assisted solvothermal method,[19] nanofiber by electrospinning,[20, 21] nanoflower by hydrothermal method,[22] nanosphere by solvothermal method,[23] and nanoparticle by plasma-enhanced chemical vapor deposition.[24] Among them, hydrothermal synthesis has its unique advantages compared with other methods, and its simple equipment requirements make the whole process easier to operate and industrial realization. The uniformity and controllability of products give material more suitable morphology to achieve higher response or lower detection limit. Meanwhile, hydrothermal synthesis process also allows surface modification and uniform doping, which are two typical ways to improve sensing performance, as has been reported.[25, 26]

In this work, we prepared pompon-like Co_3O_4 via hydrothermal

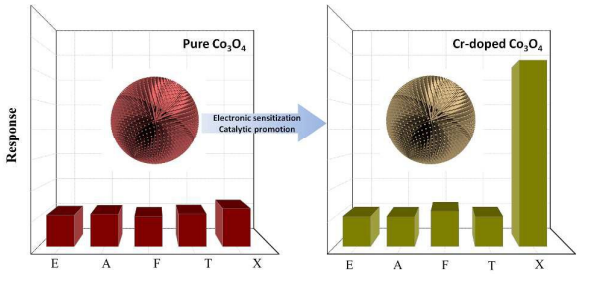

Fig.1 Performance comparison between pure Co_3O_4 and Cr-doped Co_3O_4 sensor. (E stands for ethanol, A stands for acetone, F stands for formaldehyde, T stands for toluene, and X for xylene. All gas was detected at 5 ppm.)

[a] College of Electronic Science and Engineering, Jilin University, Changchun 130012, China. Email: ruansp@jlu.edu.cn.
[b] State Key Laboratory on Integrated Optoelectronics, Jilin University, Changchun 130012, China. Email: xindong@jlu.edu.cn.
[c] Institute of Metal Research, Chinese Academy of Sciences, Shenyang, 110016, China.

Electronic Supplementary Information (ESI) available: [details of any supplementary information available should be included here]. See DOI: 10.1039/x0xx00000x

synthesis, the topography of which provides a large surface area, and the different proportions of Cr doping have been conducted to enhance material's sensing properties. Both of large surface area and Cr-doping are considered to provide more active spots, where the oxidation reaction between material and target gas carries out readily or vigorously. To investigate the best doping ratio, a series of experiments with different proportion of Cr doping has been implemented. As for the effect of Cr-doping, it is considered that the gas-sensing properties of prepared material benefit a lot from its catalytic oxidation of methyl groups.

2. Experimental Section

2.1 Chemical reagents

Cobaltous acetate tetrahydrate ($Co(CH_3COO)_2{\cdot}4H_2O$, Xilong Chemical Reagent Co.), L-Lysine ($C_6H_{14}N_2O_2$, China, the Chemical Reagent Co., Ltd.), Chromium (III) 2,4-pentanedionate ($Cr(C_5H_7O_2)_3$, Xiya Reagent Research Center), anhydrous ethanol (CH_3CH_2OH, Beijing Chemicals Co.). All of these chemicals were analytic grade and used without any further purification.

2.2 Preparation of pompon-like Co_3O_4 and Cr-doped Co_3O_4 hierarchical nanostructures

The undoped Co_3O_4 hierarchical nanostructures were synthesized by a hydrothermal reaction as reported with some modification.[27] Cobaltous acetate tetrahydrate (0.249 g) was dissolved in a mixture of anhydrous ethanol (45 mL) and deionized water (5 mL). After adding L-lysine (0.292 g), the solution was homogenized by ultrasonic transduction for 5 min. Then the precursor solution was transferred into a Teflon-lined stainless steel autoclave with a volume of 100 mL, which was heated and maintained at 180 °C for 10 h. When cooling down to the room temperature, the resulting product was centrifuge and washed several times with ethanol until the supernatant was almost colorless, and then dried at 60 °C for 24 h, after which the resulting product showed a contour of spherical flowers. The obtained powders were calcined at 600 °C for 2 h, and transferred into pompon-like hierarchical nanostructures.

In order to investigate the effect of Cr doping on the gas sensing performance, a series of different proportions of Cr were added into the precursor solution, ranging from 1 at% to 7 at% (Cr/Co=1, 2, 3, 4, 5, 6 and 7 at%), and the resulting products had a similar appearance with as-prepared undoped Co_3O_4 hierarchical nanostructures.

2.3 Sample Characterization

X-ray diffraction (XRD) analysis was conducted on a Scintag XDS-2000 X-ray diffractometer with Cu Kα radiation (λ=1.5418 Å). X-ray photoelectron spectroscopy (XPS) data was obtained from VG ESCALAB MK Ⅱ spectrometer with an Mg KR excitation (1253.6 eV). Scanning electron microscopy (SEM) was performed on a SHIMADZU SSX-550 (Japan) instrument. Surface area and pore size distribution were evaluated using Brunauer-Emmett-Teller (BET) and Barrett-Joyner-Halenda (BJH) methods, respectively, and the data of surface area were obtained from a Micromeritics Gemini VII 2390 instrument.

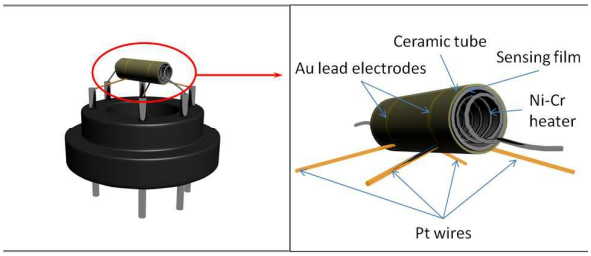

Fig.2 The schematic structure of gas sensor.

2.4 Sensor fabrication and measurement

The alumina ceramic tube (length = 4 mm, external diameter = 1.2 mm, internal diameter = 0.6 mm) with two ring-like Au electrodes on its surface (electrodes width = 0.65 mm, separation = 0.2 mm) was used for gas sensors.

The fabrication process of gas sensor is as follows: the as-prepared sample was mixed with deionized water at a weight ratio of 4:1 to shape a paste. Then the paste was coated on a ceramic tube to form a sensing film (with a thickness of about 300 μm). The ceramic tube has two Au electrodes previously printed, each of which was attached by a Pt lead wire. A spiral heating wire made of Ni-Cr alloy was inserted through the hollow center of the ceramic tube to control the operating temperature. All the six wires' ends were welded a pedestal with six pins. The structure of the device is shown in Fig.2. The completed sensor was aged by heating it for two days.

The gas sensing performance data of fabricated sensor were obtained from the gas sensing test by a Chemical gas sensor-8 (CGS-8) intelligent gas sensing analysis system (Beijing Elite Tech Co., Ltd., China) under a room condition (17 °C, 43 RH%). The values of sensor resistance were acquired by the analysis system automatically. The detecting atmosphere is a mixture of air and target gas in a certain concentration, made by injecting saturated target gas or liquid into the test chamber of 20 L through a rubber plug with a microinjector. After being heated to be stable in air, the resistances of sensors was R_a, and while reaching a new constant value in the detecting atmosphere, the resistances were R_g. The response value (R) was defined as $R=R_g/R_a$ (P-type semiconductor). Above process was sensor's response, and then the test chamber was opened to make the sensor recover in air. The time spent by the sensor to achieve 90% of the total resistance change was defined as the response time (target gas adsorption) or the recovery time (target gas desorption).

3. Results and discussion

3.1 Characterization of Co_3O_4 and Cr-doped Co_3O_4 hierarchical nanostructures

The crystal phase of Co_3O_4 and Cr-doped Co_3O_4 hierarchical nanostructures were identified by X-ray diffraction (XRD), and all samples exhibited similar XRD patterns of the Co_3O_4 phase Co_3O_4 (JCPDS# 43-1003) (Fig.3). No secondary phase is

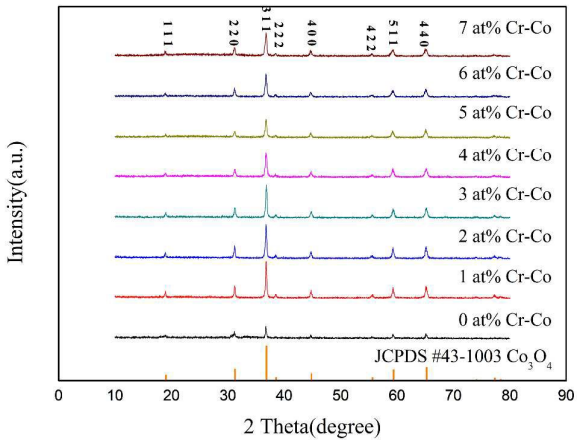

Fig.3 XRD patterns of pure and Cr-doped Co3O4 hierarchical nanostructures.

observed in the Cr-doped Co_3O_4 hierarchical nanostructures. The absence of Cr-related peaks in the Cr-doped Co_3O_4 specimens is attributed to the incorporation of Cr into the Co_3O_4 lattice, although it cannot be excluded that there are possibilities of a Cr-related secondary phase with a low crystallinity or a secondary phase below the detection limit of XRD.

In order to investigate the incorporation of Cr in Co_3O_4 and the physical and chemical state of components, the specimen was further analyzed through X-ray photoelectron spectroscopy (XPS) (Fig.4). From the curve shown as Fig.4b, it can be observed that the peak intensity centred at 781 eV and 796 eV are respectively corresponded to Co $2\mathbf{p_{1/2}}$ and Co $2\mathbf{p_{3/2}}$, whose energy difference splitting was 15.0 eV, indicting the existence of both Co^{2+} and Co^{3+}.[28] As depicted as Fig.4c, the peaks of Cr $2\mathbf{p_{1/2}}$ and Cr $2\mathbf{p_{3/2}}$ are obvious at 586.5 eV and 578.5 eV, which indicates that Cr is doped into Co_3O_4. Fig.4d shows the peak intensity of O 1s. The binding energy for C 1s peak (284.7 eV) is used as an internal reference.

The morphology and structure of specimens were observed by

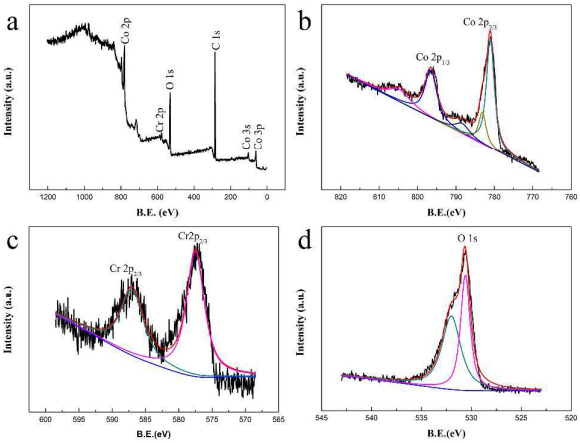

Fig.4 XPS spectra of 5 at% Cr-doped Co_3O_4 hierarchical nanostructures (a) full spectrum; (b) Co 2p; (c) Cr 2p; (d) O 1s.

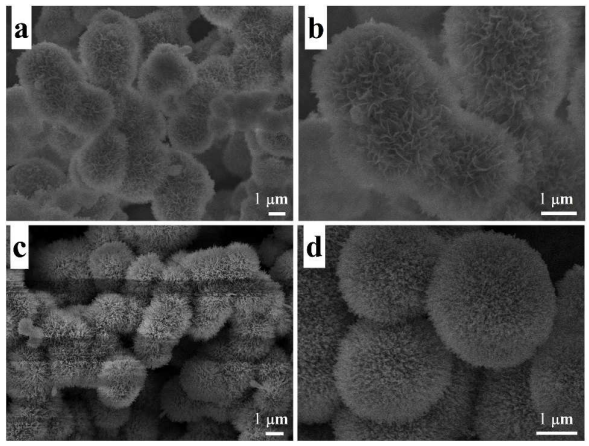

Fig.5 (a) and (b) The low-magnification and high-magnification SEM images of specimens without heat treatment; (c) and (d) The low-magnification and high-magnification SEM images of 5 at% Cr-doped Co_3O_4 hierarchical nanostructures calcined at 600 °C for 2 hours.

scanning electron microscopy (SEM). Fig.5a shows a low-magnification SEM image of precursor without heat treatment, and Fig.5b is the high-magnification SEM image. It can be observed that a flower-like structure assembled by many petals has a diameter of about 2 um. Fig.5c and Fig.5d give out low-magnification and high- magnification SEM images of specimen with a heat treatment at 600 °C, respectively, and the "flower" was converted to be a pompon-like structure with a lot of branches on the surface. As secondary structures, the petals and branches are in the size range of 50-100 nm. This hierarchical nanostructure is considered to provide porosity and increase the specific surface area. For a further confirm, the typical BET-surface area and pore size distribution of the specimen were determined by measuring the corresponding nitrogen adsorption-desorption isotherms, which are shown as Fig.6. It can be observed that the curve presents a type III isotherm with an H3 hysteresis loop at a high relative pressure, according to Brunauer-Deming-Deming-Teller (BDDT) classification, which indicates the presence of silt-like

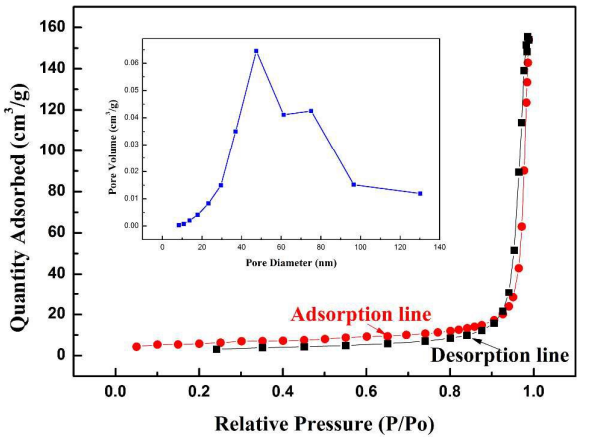

Fig.6 Typical N_2 adsorption-desorption isotherms and pore-size distribution curve (the inset) of 5 at% Cr-doped Co_3O_4 hierarchical nanostructures.

mesopores (20-120 nm) in the specimens. The specific area of specimens is determined to be 20.53 m^3/g. The vignette is the pore size distribution of the specimen, and most of pore fall into the size range of 40-60 nm.

3.2 Gas-sensing performance

It is acknowledged that for a semiconductor sensor, the response to gas is usually dependent on the operating temperature. The responses to 5 ppm xylene of all the sensors were tested at different temperatures from 80 °C to 210 °C, and the changing trends were depicted as Fig.8a. The sensor based on pure Co_3O_4 reaches the highest response to 5 ppm xylene at 161 °C, and the responses of all the sensors based on Cr-doped Co_3O_4 have a tendency to rise before falling, and the temperature of 139 °C was taken as the cut-off point, so the optimum temperature of sensor based on pure Co_3O_4 was

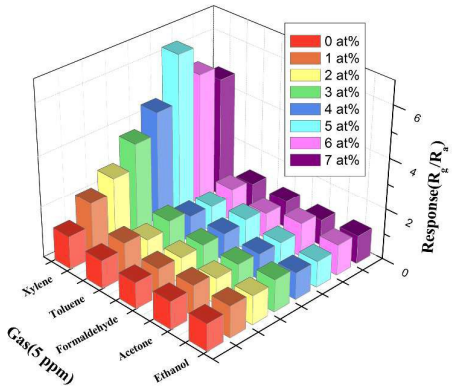

Fig.7 Responses to 5 ppm various gases of sensors based on pure and different Cr-doped Co_3O_4 at their optimum operating temperature.

Table 1 Response and selectivity of sensors based on pure and different Cr-doped Co_3O_4 at their optimum operating temperature.

Ratio of Cr	Operating Temperature (°C)	R1	R2	S (R1/R2)
0 at%	161	1.29	1.10 (T)	1.17
1 at%	139	2.18	1.33 (T)	1.64
2 at%	139	2.75	1.13 (E)	2.43
3 at%	139	3.69	1.30 (T)	2.84
4 at%	139	4.53	1.07 (F)	4.23
5 at%	139	6.38	1.20 (F)	5.32
6 at%	139	5.25	1.32 (A)	3.98
7 at%	139	4.69	1.1 (T,E)	4.26

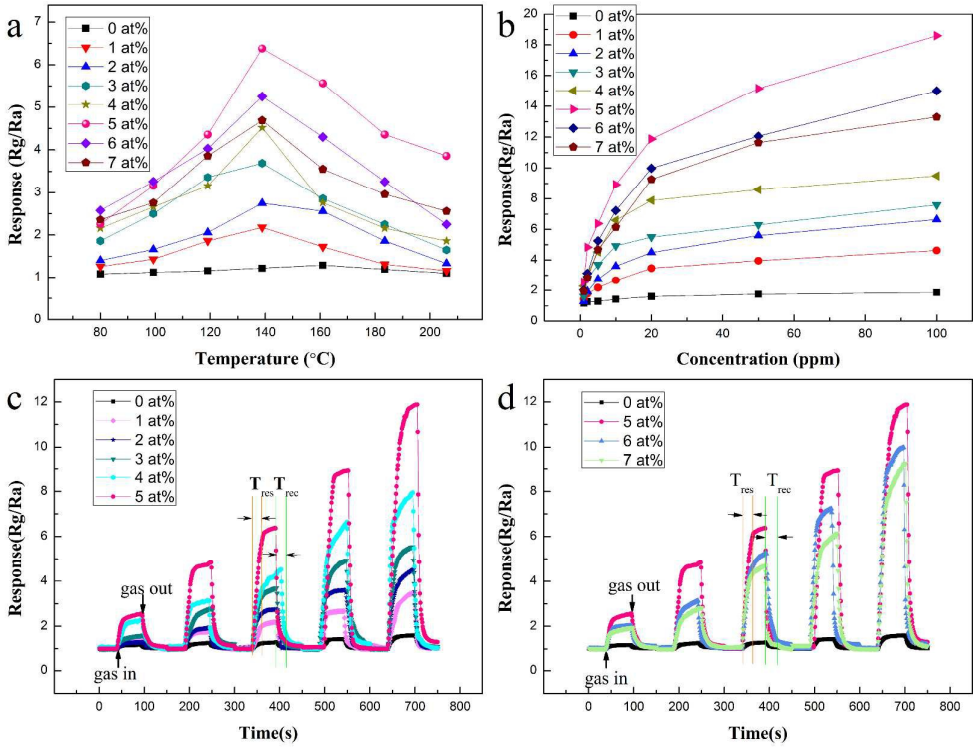

Fig.8 (a) Response of sensors based on as-prepared hierarchical nanostructures to 5 ppm xylene as a function of the operating temperature; (b) Response of sensors versus different xylene concentration at their optimum operating temperature; (c) and (d) Response transients of sensors varying from 1 ppm to 100 ppm xylene.

Table 2 Response and selectivity of sensors based on pure and different Cr-doped Co_3O_4 at their optimum operating temperature.

No.	Materials	Concentration	Temp. (℃)	Response	Ref.
1	Co_3O_4 nanocubes	100 ppm (xylene)	200	6.45	19
2	CuO flowers	1000 ppm (xylene)	260	3.6	29
3	C-doped WO_3 nanofibers	50 ppm (xylene)	370	199	30
4	Pd functionalized WO_3 nanowires	1000 ppm (xylene)	300	2.65	31
5	Rh-catalyzed WO_3 hollow spheres	20 ppb (p-xylene)	400	1.49	32
6	SnO_2 doped WO_3 hollow microspheres	100 ppm (xylene)	300	46.91	33
7	Pd-loaded SnO_2 yolk-shell	5 ppm (o-xylene)	350	17.1	34
8	Ag@SnO_2 core-shell NPs	5 ppm (p-xylene)	300	16.17	35
9	Mixed SnO_2 NPs and MWCNTs	3.6 ppm (xylene)	380	8.64	36
10	Au@NiO yolk-shell NPs	5 ppm (p-xylene)	350	7.93	37
11	Mesoporous α-Fe_2O_3 nanostructures	1000 ppm (xylene)	340	17.54	38
12	Cr-doped Co_3O_4 hierarchical nanostructures	5 ppm (xylene)	139	6.38	This work

determined to be 161 °C, and all the sensors based on Cr-doped Co_3O_4 was 139 °C. Then at respective optimum temperature, responses to 5 ppm toluene, formaldehyde, ethanol, and acetone etc. were measured to determine the selectivity of sensors (Fig.7). Among the different gases, all the sensors showed higher response to xylene than others, and as for the selectivity (the ratio of the highest response and the second high response), detail were listed as Table1. "R1" stands for the highest response (to xylene), and "R2" for the second response. In "R2" column, T is for toluene, E is for ethanol, F is for formaldehyde, and A for acetone. Compared with pure Co_3O_4, every Cr-doped Co_3O_4 has an improvement in selectivity. On the other hand, with the increasing of ratio of Cr, response to xylene of sensors has a tendency to rise before falling, and when the ratio of Cr is 5 at%, both of sensor's response to xylene and selectivity has a maximum increasing. So the 5 at% is determined to be the best ratio of Cr-doping. The optimum temperature and response were compared with some reports already published to have response to xylene, shown as Table 2.

The response and recovery behaviour is also a significant property for gas sensor. The response and recovery processes of different sensors in different concentration gas are shown as Fig.8c and Fig.8d. All the response reached the constant value fast, and step shaped obviously. All response times (T_{res}) are in the range of 15~30 s, and recovery times (T_{rec}) in the range of 10~30 s, which indicate the pure and Cr-doped Co_3O_4 has a preeminent response-recovery property.

For finding out the relationship between the response value and the gas concentration, all the sensors were evaluated in different xylene concentrations ranging from 1 ppm to 100 ppm, as presented in Fig.8b. The responses rise sharply in the concentration range of 1-20 nm, and this near linear increase tells the superiority of sensors in the low concentration measurement. When the xylene concentration exceeds 20 ppm, the responses of sensors almost tend to saturate gradually, and the responses have a slow rising or even flat slope over 20 ppm, and in the range below 20 ppm, an approximate linear relationship (y=1.9512x+0.7682) between the response and xylene concentration was observed. The detection limit of xylene for the sensor based on 5 at% Cr-doped Co_3O_4 hierarchical nanostructures is 1.15 ppm, when the criterion for gas detection is set to Rg/Ra>3.[39] All above states clear that sensors based on Cr-doped Co_3O_4 hierarchical

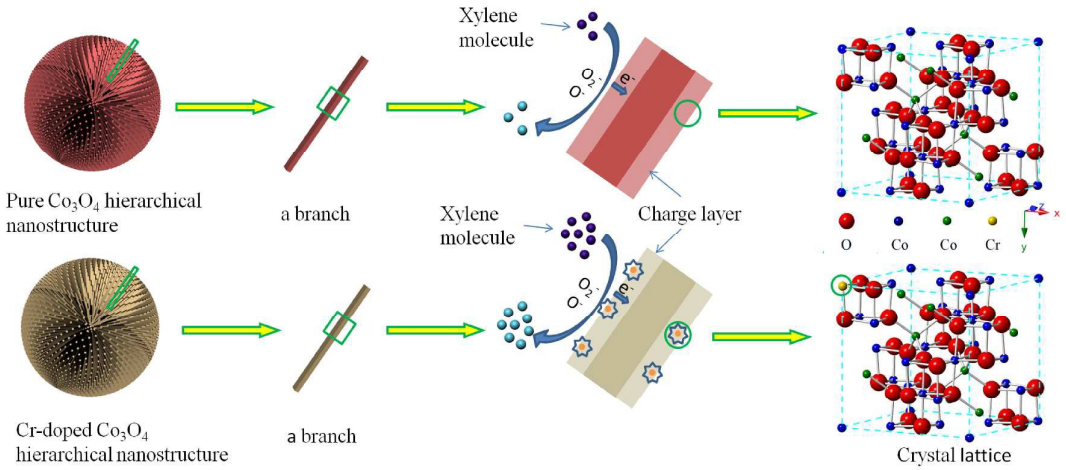

Fig.9 Diagram illustrating the influence of chromium substitution of cobalt lattice dispersed Co_3O_4 phase on the area of intergrain contacts.

nanostructures are more suitable for the test in the low concentration range of 1-20 ppm.

3.3 Possible gas-sensing mechanism

Typically, the sensing mechanism can be explained through the theory of resistance change of the sensor caused by the adsorption and desorption of gas molecules on the surface of sensing material. When the sensor based on Cr-doped Co_3O_4 is exposed in air, oxygen molecules will adsorb onto the surface of Cr-doped Co_3O_4 material to generate chemisorbed oxygen species (O_2^- ,O^- and O^{2-}) by capturing electrons from sensing material, so one effect of aging process is to make sensor into the normalization, a stable state of sensing material whose surface adsorbs oxygen ions in air. When sensor is surrounded by detecting gas, the chemisorbed oxygen species will react with the gas molecules, the process of which is accompanied with electronic gain and loss, and the resistance of sensor changes to shape a response step. The greater the amount of electronic gain and loss is, the higher the response is. The reaction equations involved in above process are listed as followed:

$$O_{2(gas)} \leftrightarrow O_{2(ads)} \quad (1)$$

$$O_{2(ads)} + e^- \leftrightarrow O^-_{2(ads)} \quad (2)$$

$$O^-_{2(ads)} + e^- \leftrightarrow 2O^-_{(ads)} \quad (3)$$

$$O^-_{(ads)} + e^- \leftrightarrow O^{2-}_{(ads)} \quad (4)$$

Co_3O_4 is a typical p-type semiconductor, whose main carrier is holes, and the resistance decrease with the increase of holes concentration. The adsorption of negatively charged oxygen on the surface at sensing temperature induces the accumulation of holes near the sensor surface. Under this configuration, when sensor is exposed to a reducing analyte gas, the reducing gas is oxidized by negatively charged oxygen, thus conduction occurs along the conductive shell layers.

In general, a variety of gases will react with oxygen ions, so the pure and Cr-doped Co_3O_4 responded to many gases. But to xylene, the response of Cr-doped Co_3O_4 stands out, for the reason that the entre of Cr introduces active centres, which promoted the reaction between oxygen ions and xylene molecules depicted as Fig.9, familiar to the Zn-doped SnO_2,[40] and the catalyst oxidation of methyl groups by Cr-doping had been reported.[41] About the substitution of Cr at the site of Co^{3+}, it has to be mentioned that the ionic size of Cr^{3+} (0.615 Å) at the coordination number (CN) of 6 is approximately equal to the size of Co^{3+} (0.610 Å or 0.545 Å) at CN=6. When xylene was introduced, there may be the following reactions occurring on the surface of Cr-doped Co_3O_4:

$$CH_3C_6H_5CH_3 + O^-_{(ads)} \xrightarrow{Cr-Co_3O_4} CH_3C_6H_5CH_2OH + e^- \quad (5)$$

$$CH_3C_6H_5CH_2OH + O^-_{(ads)} \xrightarrow{Cr-Co_3O_4} CH_2OHC_6H_5CH_2OH + e^- \quad (6)$$

The chemisorbed oxygen species would react with the xylene under the catalysis effect of Cr-doped Co_3O_4, and the electrons captured by the chemisorbed oxygen species were returned to sensing material. Consequently, the recombination between electrons and holes increased the resistance.

4. Conclusions

Pompon-like Pure and Cr-doped Co_3O_4 hierarchical nanostructures were synthesized, characterized, and utilized for the fabrication of xylene-sensing sensor. The effect of proportion of Cr was investigated, and measurement result showed 5 at% (Cr/Co) was the optimum ratio, under which, the Pompon-like Cr-doped Co_3O_4 hierarchical nanostructures reached the highest response to 5 ppm xylene. The doping of Cr induced a significant enhancement on the detection of xylene, which also improved the selectivity of material compared with pure Co_3O_4 hierarchical nanostructures. In short, the presently constructed Cr-doped Co_3O_4 hierarchical nanostructures have a potential in the application of xylene sensor.

Acknowledgements

This work was supported by the National Natural Science Foundation of China (Grant Nos. 61404058 and 11574110), Project of Science and Technology Plan of Changchun City (Grant No. 14KG020) and Opened Fund of the State Key Laboratory on Integrated Optoelectronics (No. IOSKL2013KF10).

Notes and references

1 M. Gérin, J. Siemiatycki, M. Désy and D. Krewski, *Am. J. Ind. Med.*, 1998, **34**, 144-156.
2 P. Nizamidin, A. Yimit, I. Nurulla and K. Itoh, *ISRN Spectroscopy*, 2012, **2012**, 1-6.
3 M. Girschikofsky, M. Rosenberger, S. Belle, M. Brutschy, S. R. Waldvogel and R. Hellmann, *Sens. Actuators B Chem.*, 2012, **171-172**, 338-342.
4 B. Applegate, S. Kehrmeyer and G. Sayler, *Appl. Environ. Microbiol.*, 1998, **64**, 2730-2735.
5 K.-Y. Choi, J.-S. Park, K.-B. Park, H. J. Kim, H.-D. Park and S.-D. Kim, *Sens. Actuators B Chem.*, 2010, **150**, 65-72.
6 T. Baimpos, L. Gora, V. Nikolakis and D. Kouzoudis, *Sens. Actuators A Phys.*, 2012, **186**, 21-31.
7 S. J. Pearton, F. Ren, Y.-L. Wang, B. H. Chu, K. H. Chen, C. Y. Chang, W. Lim, J. Lin and D. P. Norton, *Prog. Mater. Sci.*, 2010, **55**, 1-59.
8 D. Wang, Q. Wang and T. Wang, *Inorg. Chem.*, 2011, **50**, 6482-6492.
9 D. Wang, Y. Yu, H. He, J. Wang, W. Zhou and H. D. Abruña, *ACS Nano*, 2015, **9**, 1775-1781.
10 W. Hao, S. Chen, Y. Cai, L. Zhang, Z. Li and S. Zhang, *J. Mater. Chem. A*, 2014, **2**, 13801-13804.
11 X. Xia, J. Tu, Y. Zhang, X. Wang, C. Gu, X.-b. Zhao and H. J. Fan, *ACS Nano*, 2012, **6**, 5531-5538.
12 T. Maruyama and S. Arai, *J. Electrochem. Soc.*, 1996, **143**, 1383-1386.
13 L.-J. Zhou, Y. Zou, G.-D. Li, X. Zou, J. Zhao, M. Fan, Y. Liu and D. Wang, *RSC Advances*, 2014, **4**, 22951.
14 F. Li, J. Chen, Q. Zhang and Y. Wang, *Green Chem.*, 2008, **10**, 553.
15 X. Zhou, Z. Xia, Z. Tian, Y. Ma and Y. Qu, *J. Mater. Chem. A*, 2015, **3**, 8107-8114.

16 K. Deori and S. Deka, *CrystEngComm*, 2013, **15**, 8465.
17 L. F. Liotta, H. Wu, G. Pantaleo and A. M. Venezia, *Catal. Sci. Technol.*, 2013, **3**, 3085.
18 S. Moon, N. M. Vuong, D. Lee, D. Kim, H. Lee, D. Kim, S.-K. Hong and S.-G. Yoon, *Sens. Actuators B Chem.*, 2016, **222**, 166-172.
19 C. Sun, X. Su, F. Xiao, C. Niu and J. Wang, *Sens. Actuators B Chem.*, 2011, **157**, 681-685.
20 Q. Feng, X. Li, J. Wang and A. M. Gaskov, *Sens. Actuators B Chem.*, 2016, **222**, 864-870.
21 F. Qu, C. Feng, C. Li, W. Li, S. Wen, S. Ruan and H. Zhang, *Int. J. Appl. Ceram. Technol.*, 2014, **11**, 619-625.
22 L. T. Hoa, J. S. Chung and S. H. Hur, *Sens. Actuators B Chem.*, 2016, **223**, 76-82.
23 J. Park, X. Shen and G. Wang, *Sens. Actuators B Chem.*, 2009, **136**, 494-498.
24 D. Barreca, D. Bekermann, E. Comini, A. Devi, R. A. Fischer, A. Gasparotto, M. Gavagnin, C. Maccato, C. Sada, G. Sberveglieri and E. Tondello, *Sens. Actuators B Chem.*, 2011, **160**, 79-86.
25 L. Zhu, D. Zhang, Y. Wang, C. Feng, J. Zhou, C. Liu and S. Ruan, *RSC Advances*, 2015, **5**, 28105-28110.
26 Y. Lin, W. Wei, Y. Li, F. Li, J. Zhou, D. Sun, Y. Chen and S. Ruan, *J. Alloy. Compd.*, 2015, **651**, 690-698.
27 S. J. Hwang, K. I. Choi, J. W. Yoon, Y. C. Kang and J. H. Lee, *Chemistry*, 2015, **21**, 5872-5878.
28 J. Xu, P. Gao and T. S. Zhao, *Energy Environ. Sci.*, 2012, **5**, 5333-5339.
29 C. Yang, F. Xiao, J. Wang and X. Su, *Sens. Actuators B Chem.*, 2015, **207**, 177-185.
30 L. Deng, X. Ding, D. Zeng, S. Zhang and C. Xie, *Sens. J., IEEE*, 2012, **12**, 2209-2214.
31 F. Chávez, G. F. Pérez-Sánchez, O. Goiz, P. Zaca-Morán, R. Peña-Sierra, A. Morales-Acevedo, C. Felipe and M. Soledad-Priego, *Appl. Surf. Sci.*, 2013, **275**, 28-35.
32 K.-I. Choi, S.-J. Hwang, Z. Dai, Y. C. Kang and J.-H. Lee, *RSC Advances*, 2014, **4**, 53130-53136.
33 Y. Gui, F. Dong, Y. Zhang, Y. Zhang and J. Tian, *Mat. Sci. Semicon. Proc.*, 2013, **16**, 1531-1537.
34 Y. J. Hong, J. W. Yoon, J. H. Lee and Y. C. Kang, *Chemistry*, 2014, **20**, 2737-2741.
35 P. Rai, S. M. Majhi, Y.-T. Yu and J.-H. Lee, *RSC Advances*, 2015, **5**, 17653-17659.
36 K.-Y. Choi, J.-S. Park, K.-B. Park, H. J. Kim, H.-D. Park and S.-D. Kim, *Sens. Actuators B Chem.*, 2010, **150**, 65-72.
37 P. Rai, J. W. Yoon, H. M. Jeong, S. J. Hwang, C. H. Kwak and J. H. Lee, *Nanoscale*, 2014, **6**, 8292-8299.
38 Y. Li, Y. Cao, D. Jia, Y. Wang and J. Xie, *Sens. Actuators B Chem.*, 2014, **198**, 360-365.
39 F. Qu, Y. Wang, Y. Wang, J. Zhou and S. Ruan, *RSC Advances*, 2014, **4**, 24211.
40 Y. Wang, D. Jiang, W. Wei, L. Zhu, L. Shen, S. Wen and S. Ruan, *RSC Advances*, 2015, **5**, 50336.
41 H. J. Kim, J. W. Yoon, K. I. Choi, H. W. Jang, A. Umar and J. H. Lee, *Nanoscale*, 2013, **5**, 7066-7073.

Graphical Abstract:

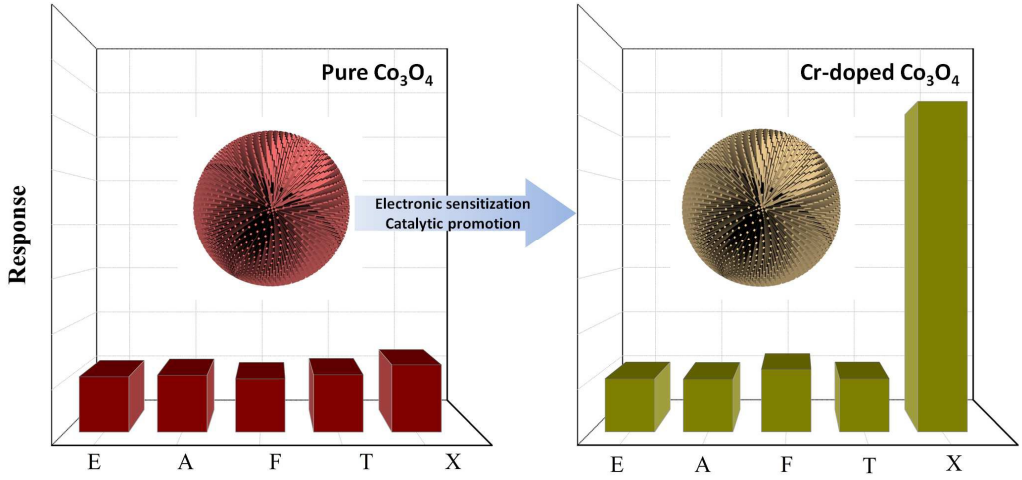

Unique pompon-like Cr-doped Co_3O_4 hierarchical nanostructures were prepared via hydrothermal method, showing extraordinary sensing properties to xylene.